2004-12

Alternate configurations for blocked impurity band detectors

Garcia, Jonathan C.

Monterey California. Naval Postgraduate School

NAVAL POSTGRADUATE SCHOOL

MONTEREY, CALIFORNIA

THESIS

ALTERNATE CONFIGURATIONS FOR BLOCKED IMPURITY BAND DETECTORS

by

Jonathan C. Garcia

December 2004

Thesis Advisor:	Nancy M. Haegel
Co-Advisor:	Gamani Karunasiri

Approved for public release; distribution is unlimited

THIS PAGE INTENTIONALLY LEFT BLANK

REPORT DOCUMENTATION PAGE			Form Approved OMB No. 0704-0188
Public reporting burden for this collection of information is estimated to average 1 hour per response, including the time for reviewing instruction, searching existing data sources, gathering and maintaining the data needed, and completing and reviewing the collection of information. Send comments regarding this burden estimate or any other aspect of this collection of information, including suggestions for reducing this burden, to Washington headquarters Services, Directorate for Information Operations and Reports, 1215 Jefferson Davis Highway, Suite 1204, Arlington, VA 22202-4302, and to the Office of Management and Budget, Paperwork Reduction Project (0704-0188) Washington DC 20503.			
1. AGENCY USE ONLY *(Leave blank)*	**2. REPORT DATE** December 2004	**3. REPORT TYPE AND DATES COVERED** Master's Thesis	
4. TITLE AND SUBTITLE: Alternate Configurations for Blocked Impurity Band Detectors		**5. FUNDING NUMBERS**	
6. AUTHOR: Jonathan C. Garcia			
7. PERFORMING ORGANIZATION NAME(S) AND ADDRESS(ES) Naval Postgraduate School Monterey, CA 93943-5000		**8. PERFORMING ORGANIZATION REPORT NUMBER**	
9. SPONSORING /MONITORING AGENCY NAME(S) AND ADDRESS(ES) N/A		**10. SPONSORING/MONITORING AGENCY REPORT NUMBER**	
11. SUPPLEMENTARY NOTES The views expressed in this thesis are those of the author and do not reflect the official policy or position of the Department of Defense or the U.S. Government.			
12a. DISTRIBUTION / AVAILABILITY STATEMENT Approved for public release; distribution is unlimited		**12b. DISTRIBUTION CODE**	

13. ABSTRACT (maximum 200 words)

Silicon Blocked Impurity Band (BIB) detectors are highly efficient, radiation-hardened photodetectors that operate in the range of 5-40 μm. To further extend BIB coverage to 40-350 μm, Ge and GaAs BIB detectors are under development; however, these new detectors face fabrication issues that have delayed their introduction. This thesis will describe the use of a numerical model to examine alternate operating modes for GaAs BIB detectors in order to bypass current fabrication issues. The numerical simulations provide an understanding of the fundamental physics that governs detector transport. The proposed alternatives to standard operation are created by reversing the detector's bias and varying the blocking layer thickness. Modeling indicates that reversing the bias on these detectors provides a larger signal current than standard configurations, while preserving the principal benefits gained from a multilayered device. At the same time, the alternate bias configuration allows for the use of thicker blocking layers, while preserving overall detector responsivity and reducing shot noise. This proposed new model of operation should allow for the relaxation of fabrication constraints without sacrificing the inherent benefits associated with BIB detectors. These devices are of potential interest for missile defense and terahertz surveillance applications.

14. SUBJECT TERMS Blocked Impurity Band (BIB), Impurity Band Conduction (IBC), infrared detector, infrared sensors, long wavelength infrared (LWIR), very long wavelength infrared (VLWIR)			**15. NUMBER OF PAGES** 63
			16. PRICE CODE
17. SECURITY CLASSIFICATION OF REPORT Unclassified	**18. SECURITY CLASSIFICATION OF THIS PAGE** Unclassified	**19. SECURITY CLASSIFICATION OF ABSTRACT** Unclassified	**20. LIMITATION OF ABSTRACT** UL

NSN 7540-01-280-5500

Standard Form 298 (Rev. 2-89)
Prescribed by ANSI Std. 239-18

THIS PAGE INTENTIONALLY LEFT BLANK

Approved for public release; distribution unlimited

ALTERNATE CONFIGURATIONS FOR BLOCKED IMPURITY BAND DETECTORS

Jonathan C. Garcia
Lieutenant Commander, United States Navy
B.S., United States Naval Academy, 1995

Submitted in partial fulfillment of the
requirements for the degree of

MASTER OF SCIENCE IN APPLIED PHYSICS

from the

NAVAL POSTGRADUATE SCHOOL
December 2004

Author: Jonathan C. Garcia

Approved by: Professor Nancy M. Haegel
Thesis Advisor

Professor Gamani Karunasiri
Co-Advisor

Professor James H. Luscombe
Chairman, Department of Physics

THIS PAGE INTENTIONALLY LEFT BLANK

ABSTRACT

Silicon Blocked Impurity Band (BIB) detectors are highly efficient, radiation-hardened photodetectors that operate in the range of 5-40 μm. To further extend BIB coverage to 40-350 μm, Ge and GaAs BIB detectors are under development; however, these new detectors face fabrication issues that have delayed their introduction. This thesis will describe the use of a numerical model to examine alternate operating modes for GaAs BIB detectors in order to bypass current fabrication issues. The numerical simulations provide an understanding of the fundamental physics that governs detector transport. The proposed alternatives to standard operation are created by reversing the detector's bias and varying the blocking layer thickness. Modeling indicates that reversing the bias on these detectors provides a larger signal current than standard configurations, while preserving the principal benefits gained from a multilayered device. At the same time, the alternate bias configuration allows for the use of thicker blocking layers, while preserving overall detector responsivity and reducing shot noise. This proposed new model of operation should allow for the relaxation of fabrication constraints without sacrificing the inherent benefits associated with BIB detectors. These devices are of potential interest for missile defense and terahertz surveillance applications.

THIS PAGE INTENTIONALLY LEFT BLANK

TABLE OF CONTENTS

THIS PAGE INTENTIONALLY LEFT BLANK

LIST OF FIGURES

THIS PAGE INTENTIONALLY LEFT BLANK

LIST OF TABLES

THIS PAGE INTENTIONALLY LEFT BLANK

ACKNOWLEDGMENTS

First, I would like to thank the staff and facility at the Naval Postgraduate School. I am forever indebted to my instructors for their efforts and their endless patience.

I would like to thank my thesis advisor, Professor Nancy Haegel, for all of her efforts and guidance. The high standards encouraged by Professor Haegel truly enriched my time at NPS and will leave an indelible mark on both my professional and academic careers. Most importantly, I will leave Professor Haegel's tutelage understanding that if I already have the answer, then it is not really research.

I would like to thank my co-advisor for this thesis, Professor Gamani Karunasiri. His thorough reviews, thoughtful insight, and helpful suggestions were invaluable to the completion of this thesis.

I would like to thank Eric Adint for his help in creating and maintaining my computer lab. His help saved me countless hours and prevented many, many headaches.

I would like to thank the Dr. Eugene Haller and Jeff Beeman of the Lawrence Berkeley National Laboratory for their thoughtful insights regarding my research.

I would like to acknowledge R. McMurray at NASA Ames, Peter Love and colleagues at Raytheon Vision Systems and A. M. White of Malvern, England. Our conversations proved invaluable while completing this thesis. This work was supported in part by NASA Grant NNG04GB82G through the Office of Space Science and by NASA Ames Research Center.

I would like to thank my wife and family for all their support and encouragement throughout my time NPS. I truly appreciated their patience and love throughout my time at NPS.

While I was writing this thesis, my thoughts and prayers were always with my friends and colleagues that are fighting terrorism in Iraq, Afghanistan, and around the world. I thank you for your sacrifice.

THIS PAGE INTENTIONALLY LEFT BLANK

I. INTRODUCTION

A. OBJECTIVES

Blocked Impurity Band (BIB) photodetectors currently provide for imaging and spectroscopy in the far infrared (FIR) range between 5 and 40 μm. Also known as Impurity Band Conduction (IBC) photodetectors, these devices were first developed in 1977 by Petroff and Stapelbroek at the Rockwell Science Center [1]. Constructed through vapor or liquid phase epitaxial growth, these detectors consist of two ohmic contacts, a heavily doped IR active layer and a thin layer of high-purity material. The active layer of the detector consists of a thin (~20-40 μm) extrinsic region with doping concentration 10-1000 times higher than typically employed in a conventional photoconductor [2]. The hopping current present in the heavily doped material is then blocked by the thin high-purity "blocking" layer. Success of BIBs as FIR detectors stems from their ability to exhibit high quantum efficiency, lower radiation sensitivity, increased photon absorption, broader wavelength response, while lacking the transient problems that plague standard photodetectors [3].

Si BIB detectors currently operate in the 15-40 μm range, while Ge BIBs are under development to extend the wavelength response to 120 μm. Uniaxial compression techniques have pushed the wavelength limits of conventional extrinsic Ge photoconductors to 220 μm; however, the material stress limits placed on a detector from compression prevent further wavelength extension [4]. The use of uniaxial compression techniques remains extremely costly and limits the size of available detector arrays, which restricts the employment of this technique to highly specialized applications. In order to extend the further available wavelengths into the 200-350 μm range, new GaAs BIB detectors have been proposed. GaAs BIBs would offer a wavelength response up to 330 μm without the complications associated with uniaxial compression techniques.

Studies were conducted in the 1960s examining the potential of n-type GaAs material in the use of photoconductors. It was found that Tellurium doped

GaAs has a ground state ionization energy of 5.7 meV and a first excited state ionization energy of 4.3 meV, which represents wavelengths of 217 μm and 286 μm respectively [5]. Unfortunately, these low ionization energies can cause an unacceptable amount of dark current when employed in standard photoconductors. The ability of BIB detectors to block this dark current makes their configuration extremely attractive.

For optimal GaAs BIB detector performance, the impurities in the blocking layer must be held below 10^{13} cm^{-3}, which can be achieved through the use of Liquid Phase Epitaxy (LPE) growth methods. This purity level was demonstrated during research conducted at the University of California, Berkeley in 2003 [6]. Growing a high purity layer next to an extrinsic active layer on a single semiconductor device has proven much more difficult. In the ideal case, the active layer in a GaAs BIBs would have n-type doping in the range of 10^{14} cm^{-3} to 10^{15} cm^{-3} and a minority doping concentration in the range of 10^{12} cm^{-3} to 10^{13} cm^{-3}. Attempts have been made to grow tellurium doped GaAs samples; however, these samples have demonstrated majority doping levels close to 10^{16} cm^{-3} and unacceptably high levels of compensation doping [7]. Problems creating GaAs BIBs through LPE also exist because of the diffusion of the doping material from the active region into the blocking region of the device. This diffusion creates a doping transition grade at the blocking to active layer interface, which can cause several negative effects on BIB performance. This grade results in a reduction of long wavelength response and a reduction in the effectiveness of the blocking layer [8]. Increasing the blocking layer thickness would alleviate this problem, but would result in a significant loss in of detector responsivity for a given bias if applied to a conventional BIB detector. In order to alleviate these limitations, this thesis explores the consequences of applying alternate bias modes on BIB devices and proposes detector configurations that could minimize the impact of manufacturing limitations for longer wavelength applications.

B. THEORY OF STANDARD BIAS OPERATION

The basic principle behind the operation of a BIB detector is the blocking of the hopping currents in the heavily doped regions of the device by the high purity layer of the device. At the same time, the device permits free carriers that have been excited into the conduction band through photo ionization to reach an ohmic contact. In the case of n-type BIBs, the IR absorbing layer consists of both a large amount of n-type dopant and a low level of residual p-type dopant. Because of this unique doping configuration, n-type BIB detectors differ from other photoconductors through their utilization of both electrons and ionized donors within the conduction process.

The detection process begins with the application of a positive voltage to the blocking layer contact. This configuration is referred to as "standard bias." The positive voltage pushes away the positive charge on the ionized donors, N_D^+, from a region of the active layer. This region, known as the depletion region, maintains its concentration of ionized acceptors, N_A^-, and neutral donors, N_D, which creates an area of negative space charge. The negative space charge establishes an electric field region (or gradient) in both the active and blocking layers of the device that serves to separate and collect any charges created through photo-ionization. The depletion region of the device deserves special consideration and is discussed in further detail below. When photons of sufficient energy are absorbed in the depletion region of the active layer, they interact with the neutral donors present, which allow electrons to jump from the impurity band into the conduction band. Once in the conduction band, the electrons are free to pass through the blocking layer and are moved to the positively biased contact by the electric field. Also affected by the electric field, the newly created ionized donors, N_D^+, drift and recombine at the opposite contact. This movement provides the current required to measure the FIR light

incident upon the detector. Figures 1 and 2 depict the basic operation of a n-type BIB detector and its charge carrier movement.

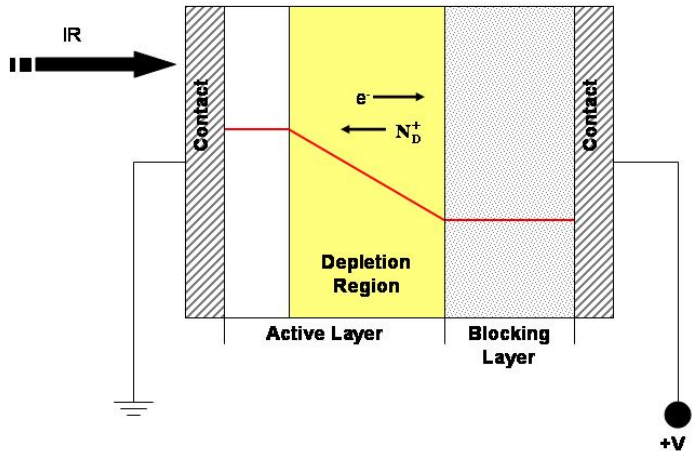

Figure 1. Schematic Diagram of N-Type BIB.

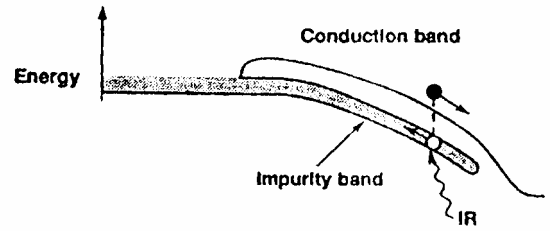

Figure 2. Energy Level Diagram for N-Type BIB ([From [09]).

The theory of a p-type BIB detectors follow the same basic operating principles described above, but with a few important variations. In this case the process begins by placing a negative voltage at blocking layer's contact. This bias creates a region of depleted of ionized acceptors N_A^- and a surplus of both positively charged ionized donors, N_D^+, and neutral acceptors. This space charge imbalance creates an electric field gradient that allows for the collection of photocurrent. In this case, an absorbed photon interacts with a neutral acceptor and creates a hole in the valence band of the detector. The hole is swept towards the negatively charged contact and passed through the blocking layer to

be collected as photocurrent. The photo ionization also creates an ionized acceptor in the impurity band of the detector that is collected and recombined at the other contact. In some ways, the operation of BIB detectors mirrors the operation of reverse bias p-n junctions. This process is depicted in Figures 3 and 4, where the red line designates the electric field profile.

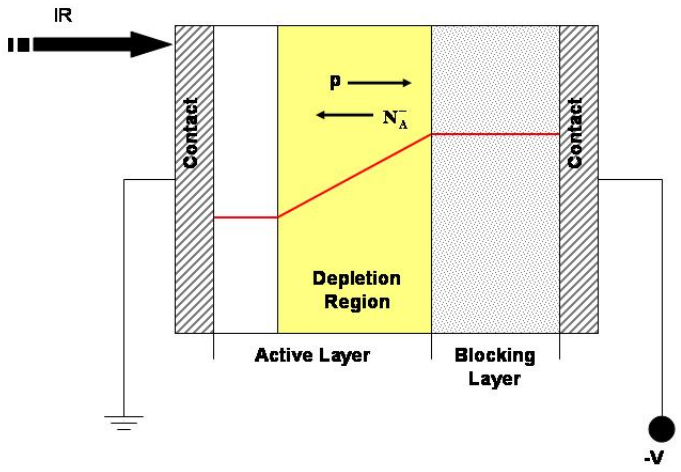

Figure 3. Schematic Diagram of P-Type BIB.

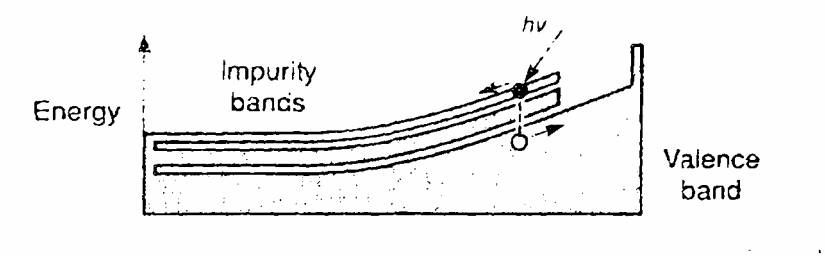

Figure 4. Energy Level Diagram for P-Type BIB (From [10]).

The depletion region of BIB detectors represents the key region for the collection of photocurrent within the device and requires a quantitative inspection. The size of the depletion region of a BIB detector depends on the amount of bias voltage applied and the concentration of minority dopant in the active layer. For our discussion, we will examine a n-type BIB. The width of the depletion region can be obtained through an application of Poisson's equation in the active layer.

$$\frac{\partial E_x}{\partial x} = \frac{\rho}{\kappa_o \varepsilon_o} = \frac{qN_A}{\kappa_o \varepsilon_o} \tag{1.1}$$

In Poisson's equation κ_o represents the semiconductor's dielectric constant and N_A represents the density of ionized acceptors. Remembering the relation between the electric field and applied voltage is $\partial V / \partial x = E_x$ (1.2), the solution for the width ***w*** of the depletion region is given by

$$w = \left[\frac{2k_o\varepsilon_o}{qN_A} |V_b| + t_B^2 \right]^{1/2} - t_B \qquad (1.3)$$

where t_B is the thickness of the blocking layer and V_B represents the applied bias voltage [11]. The peak electric field strength E_x is then represented by the following equation.

$$E_x = \frac{qN_A}{2\kappa_o\varepsilon_o}(w) \qquad (1.4)$$

The dependence of electric field strength and depletion width upon the minority acceptors concentration drives the manufacturing process of BIBs to maintain strict control over the amount of minority impurities and adds layers of difficulty to the fabrication process. These equations assume that electric field is constant in the blocking layer and a linear function inside the active layer of the device. These assumptions require a condition in which space charge does not exist in the blocking layer and is constant in the active layer. Unfortunately, these assumptions are not always valid and can lead to inaccurate results. The use of a finite difference computer code eliminates these inaccuracies and is discussed in the next chapter.

II. COMPUTER MODELING AND SIMULATION

A. BIB SIMULATION PROGRAM AND COMPUTER SUITE SETUP

The design and setup of the BIB Simulation Computer Suite (BSCS) was based on work previously completed at Fairfield University and the White Numeric Consulting Company. The BSCS consists of three individual computers that operate with the following specifications.

Operating System	Suse Linux 9.1
Processor	AMD (3000+) Athlon 64 Bit
Memory	2 GB 400 DDR RAM
Hard Drive	2 Computers with 80 GB 1 Computer with 120 GB

Table 1. BIB Computer Suite Specifications.

These computers were purchased in August, 2004 and provide a significant improvement in computational power over the legacy suite. The BSCS supports a numerical finite difference computer simulation that requires fifteen to twenty thousand iterations to produce a single solution. Programmed in FORTRAN, the BIB simulation program utilizes NAGWare F95 Revision 4.0 Compiler and the related LAPACK Numeric Libraries. This thesis required over 277 simulations, which represents approximately 2000 hours of computation.

Figure 5. The BIB Simulation Computer Suite.

B. COMPUTER MODELING OF BIB DETECTORS

The finite difference numerical simulation used to model BIB behavior calculates the steady state distribution of electric field, carrier concentration, free carrier current, and ionized impurity (hopping) current as functions of position [12]. The modeling builds on earlier work for both p-n junction devices and transient modeling of conventional photoconductors [13, 14]. In order to compute these detector characteristics, this model simultaneously solves several fundamental equations in one dimension. These equations include Poisson's equation, Continuity Equations for both positive and negative charges, the generation and recombination of holes and electrons, and a doping dependent expression for the mobility of ionized acceptors.

Since the model operates in one dimension, Poisson's equation simplifies to the following

$$\frac{\varepsilon\varepsilon_o \partial E}{\partial x} = q(p - n + N_D^+ - N_A^-) \tag{2.1}$$

where q is the fundamental charge of an electron, p and n are the respective concentration of positively and negatively charged free carriers, N_A^- is the concentration of ionized acceptors and N_D^+ is the concentration of ionized donors [15]. Along with Poisson's Equation, the simulation solves the Continuity Equation for both positively and negativity charged ionized carriers. These equations are

$$\frac{\partial p}{\partial t} = G - R - \frac{\partial J_p}{\partial x} \tag{2.2}$$

$$\frac{\partial n}{\partial t} = R - G - \frac{\partial J_N}{\partial x} \tag{2.3}$$

where the time derivatives are set to zero, G represents generation and R represents recombination of free carriers [16]. It becomes important to understand that both the J_p and the J_N are the sum of drift and diffusion currents [17].

$$\frac{J_p}{q} = p\mu_p E - D_p \frac{\partial p}{\partial x} \tag{2.4}$$

$$\frac{J_n}{q} = n\mu_n E - D_n \frac{\partial n}{\partial x} \tag{2.5}$$

To solve these equations, the model requires the mobility μ and the diffusion coefficient ***D*** for the mobile carriers within the device. Generation relates to Recombination through the following equation.

$$G - R = \left(\gamma + p\sigma\upsilon_p\right)\left(N_A - n\right) - \sigma\upsilon_p pn \tag{2.6}$$

For This equation, γ is the optical generation of free carriers, σ is capture cross section of the mobile carriers, υ_p is the effective speed of the holes across the device, and p_1 is found through an application of the mass action law [18].

$$pn \cong p_1 N_A \tag{2.7}$$

Calculating the hopping current within the detector requires special consideration. The computer model calculates hopping current by approximating the mobility of the ionized acceptors within the device. Following an approach created by Petroff and Stapelbroek, the model calculates the mobility by employing known values for both the Bohr radius a_B and the concentration of the majority carrier dopant N_A. This mobility is found through two equations, given by

$$\mu = \mu_o x^{3.5} e^{-x} \tag{2.8}$$

$$x = 2\left[N_A^{1/3} a_B\right] \tag{2.9}$$

where μ_o is a temperature dependent pre-factor [19].

In order to handle the interfaces between the different layers of a BIB detector, the computer model employs an empirically derived hyperbolic function. This hyperbolic function ensures a smooth transition of the detector's changing doping concentrations, while allowing for the control over the gradient region. The transition between two layers is represented by

$$N = \frac{N_1 + (N_2 - N_1)}{1 + e^{\left[(a-x)/g\right]}} \tag{2.10}$$

where N_1 and N_2 are the dopant concentrations of the adjoining layers, ***a*** is the position of the interface, ***x*** is the position along the detector, and ***g*** is the grading parameter [20]. The model's ability to represent the dopant grade at an interface creates a realistic depiction of the doping transitions created during the LPE growth of a detector.

Employing the equations described above, the model treats a BIB detector as a quasiambipolar system with free electrons and ionized donors for n-type devices or free holes and ionized acceptors for p-type devices [21]. To accomplish this task, the model requires the doping levels for each of the detector's layers. The front and back contacts of the device are simulated as heavily doped regions that provide free carriers at all temperatures. The model also allows for variation of the majority and minority dopant concentrations in both the active and blocking layers of the device. The model also includes variable thicknesses for all four of the detector's layers, which dictates the detector's overall length. As previously discussed, the model represents all doping transitions by employing a hyperbolic grading function. In order to handle several different photoconducting host materials, the model allows for the varying of the mobility, the hopping mobility prefactor μ_o, the Bohr radius a_B, and the ionization energy of the device's majority dopant. The model also maintains the ability to simulate various operating conditions. This is accomplished through the variation of temperature, optical generation rate γ, and applied bias. Figure 6 depicts the input file and all required variables of the computer model.

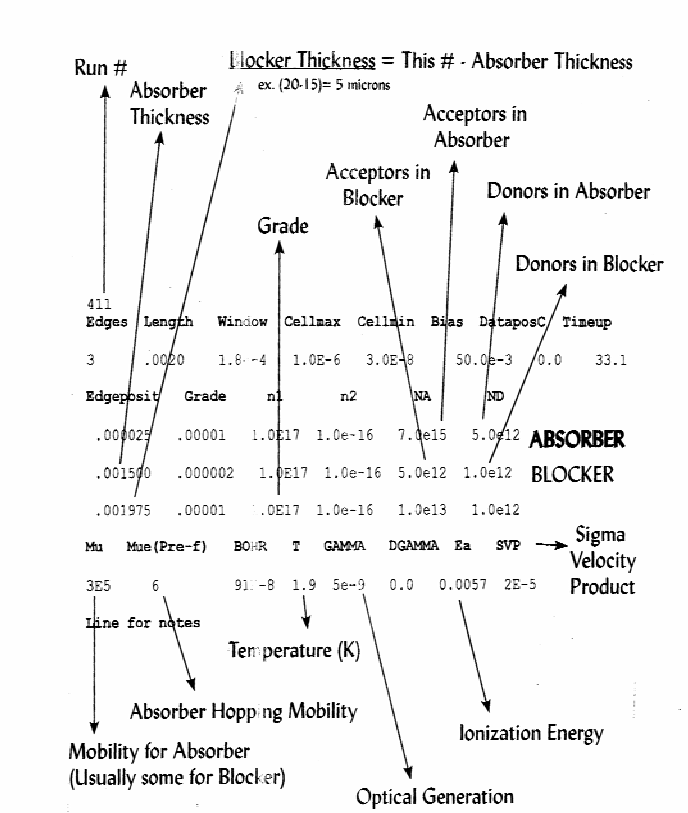

Figure 6. Data Input File for Bib Simulation Program.

The time to complete a single simulation varies with the parameters entered into the model. For instance, reducing the temperature, the optical generation rate, and the compensation doping in the active layer increases the amount of time required to complete a simulation. Due to the large number of variables within the model, the time to complete a single simulation varies from several minutes to several days. Upon completion, the model provides a single computer file that contains 13 individual data fields that are listed in Table 2. Each data field represents the spatial variation of a detector's internal distributions.

Position	Valence Band Energy
Acceptor Concentration	CPIAC
Donor Concentration	Na^- Mobility
Na^- Concentration	Electric Field
Hole Concentration	Na^- Current
Na^- Quasi Fermi Level	Hole Current
Hole Quasi Fermi Level	

Table 2. Output data fields of the BIB model for a p-type device simulation.

III. ALTERNATE BIAS CONFIGURATIONS

A. THEORY OF ALTERNATE BIAS OPERATION

To further extend BIB performance into the far IR range (40-350 μm), alternative host materials for BIBs such Ge and GaAs have been introduced with limited success. The performance of these new devices has been limited by material purity, blocking-active layer interface quality, and the lack of a reliable and reproducible method of growing an appropriately thin blocking layer. An alternate bias configuration serves to isolate and minimize many of these limitations, while maintaining acceptable charge collection characteristics. This alternate bias configuration is created by reversing the polarity of the applied bias on the detector. For a n-type device, the applied positive voltage resides on the active layer contact, which serves to push positively charged ionized donors N_D^+ towards the active to blocking layer interface of the device. For a p-type device, the applied negative voltage resides on the active layer contact, which moves the ionized acceptors N_A^- out of the active layer of the device. The alternate bias configuration forces the creation of the depletion region exclusively in the active layer. These processes are depicted in Figures 7 and 8.

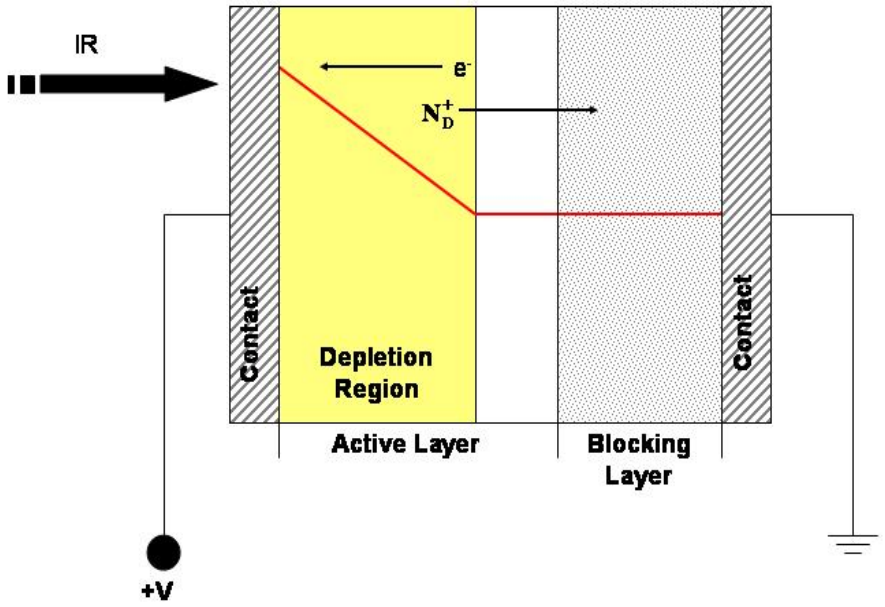

Figure 7. N-Type BIB Detector in Alternate Mode.

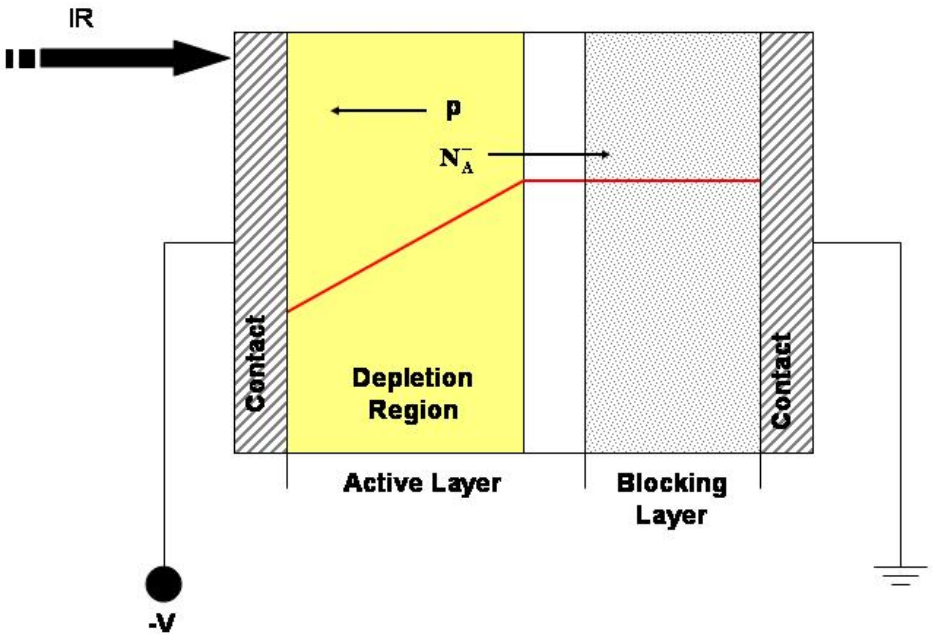

Figure 8. P-Type BIB Detector in Alternate Mode.

It is important to remember that the changing roles of the contacts facilitate the sign change of the electric field. The exclusion of the blocking layer from the depletion region raises key questions concerning the basic operation of the device. These questions include the alternate bias mode's effect on the width of the depletion region, the amount of photocurrent created by a given flux, the utility of the blocking layer, and the drift and diffusion of the free carriers present in both contact layers.

To answer these questions, the BIB computer model simulated the behavior of a standard GaAs detector that was placed under multiple biases in both modes of operation. Table 3 summarizes the parameters utilized to simulate a GaAs detector under varying bias conditions.

Absorbing Layer Majority Doping	$7x10^{15}$ cm^{-3}
Absorbing Layer Minority Doping	$5x10^{11}$ cm^{-3}
Absorbing Layer Thickness	5 μm
Blocking Layer Majority Doping	$1x10^{13}$ cm^{-3}
Blocking Layer Minority Doping	$1x10^{12}$ cm^{-3}
Blocking Layer Thickness	15 μm
Temperature	1.9 K
Applied Bias	0, ±5, ±10, ±15, ±20, ±25 ±30, ±35, ±40, ±45, ±50 ±55 mV, ±60, ±65, ±75, ±80
Bohr Radius	$91x10^{-10}$ m
Interface grade parameter	$2x10^{-6}$ cm (ideal sharp)
Contact Grade parameter	$1x10^{-5}$ cm
Optical flux rate γ	$5x10^{-9}$ s^{-1}

Table 3. GaAs modeling parameters.

Figure 9 depicts the electric field profile as a function of position for both standard and alternate bias. As expected, the alternate bias mode produces an electric field adjacent to the active layer contact and avoids significant voltage drop across the blocking layer. Consequently, the depletion regions created in the active layer by the alternate mode are larger than those created using a standard configuration. The larger depletion region allows detectors in the alternate configuration to produce higher amounts of photocurrent at a given applied voltage, which also increases the device's responsivity. These results are seen in Figure 10.

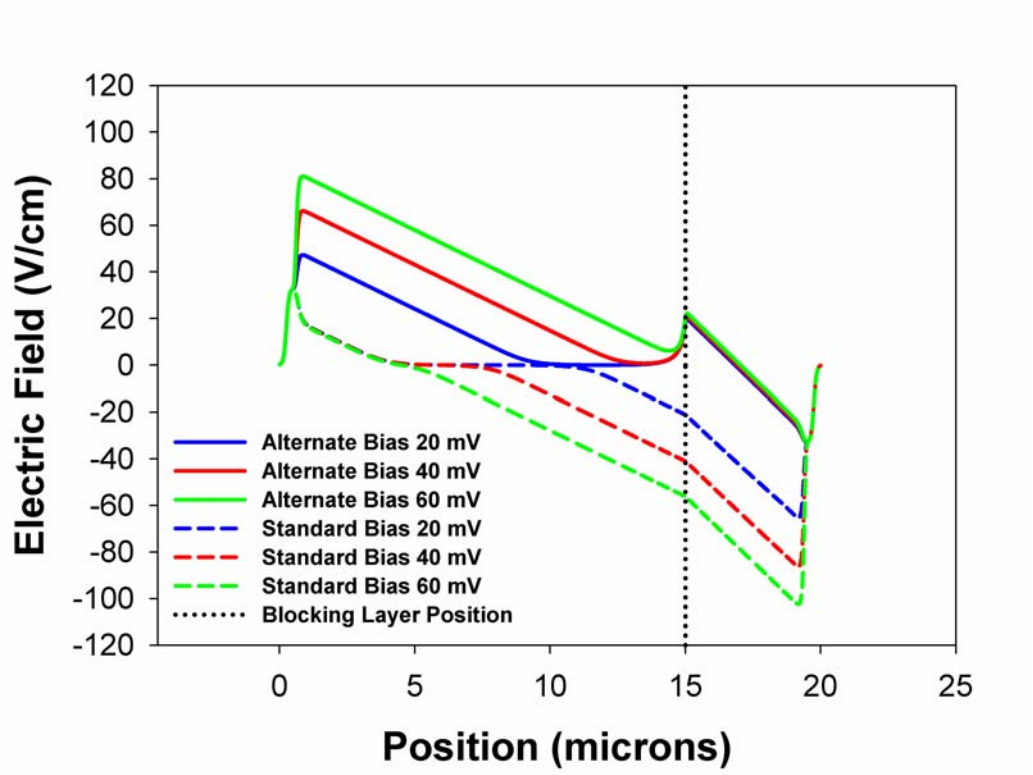

Figure 9. Electric Field as a function of Position for Varying Applied Bias.

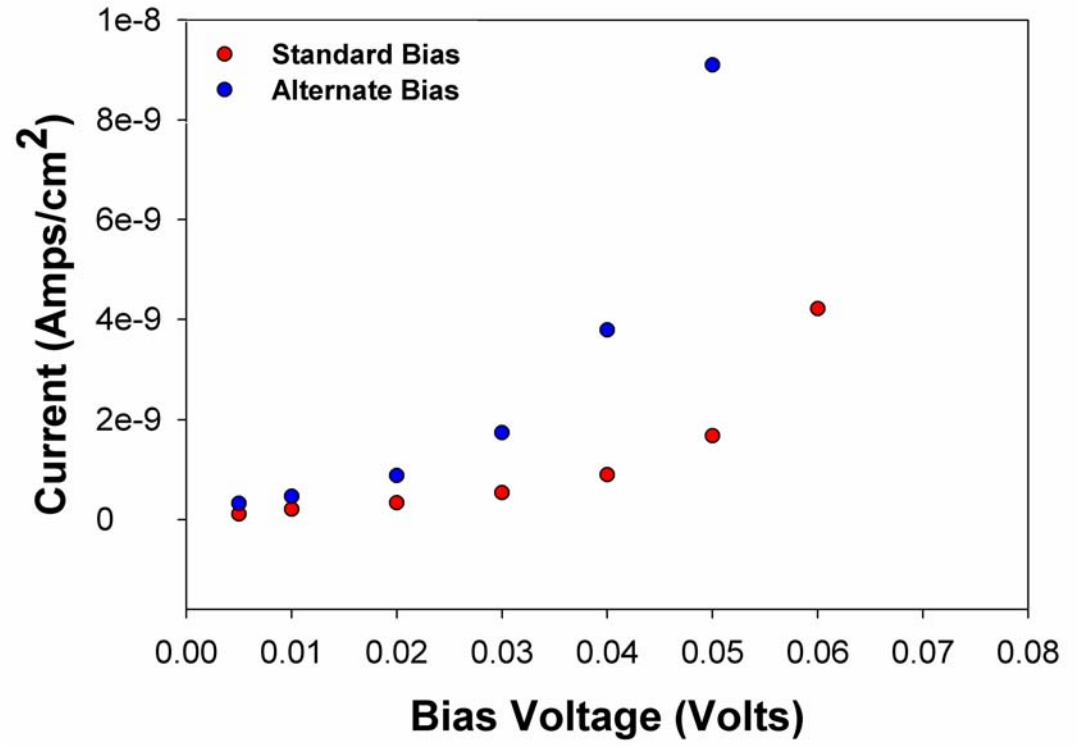

Figure 10. Total Photocurrent as a Function of Bias.

A closer examination of Figure 9 uncovers some important characteristics concerning alternate bias operation. First, a comparison of the electric field profiles between the two bias modes demonstrates the ability of an alternate bias configuration to isolate the depletion region from the interface between the blocking layer and active layer. At the same time, the gradient of the electric field remains nearly constant within the depletion region of active layer regardless of bias or bias mode. The gradient of the field reflects the net space charge ρ, where $\rho \approx N_D^+ + p - N_A^- \approx N_D^+$ (3.1) [22]. Figure 9 also shows that under alternate bias mode the electric field undergoes a sign change within the blocking layer. This sign change is a result of the changing predominance of drift and diffusion currents within the detector and will be discussed in detail in the following section. Under the alternate bias configuration, the electric field ensures that when photo-ionization occurs the subsequent electrons and ionized donors N_D^+ are swept in opposite directions along the detector. Ultimately, the electrons are collected at the active layer contact and the ionized donors stopped by the blocking layer.

Within an n-type detector, the net motion of the ionized donors N_D^+ generates the hopping current that needs to be stopped by the blocking layer. Fortunately, the BIB computer simulation allows for the separate calculation of the hopping current as a function of position.

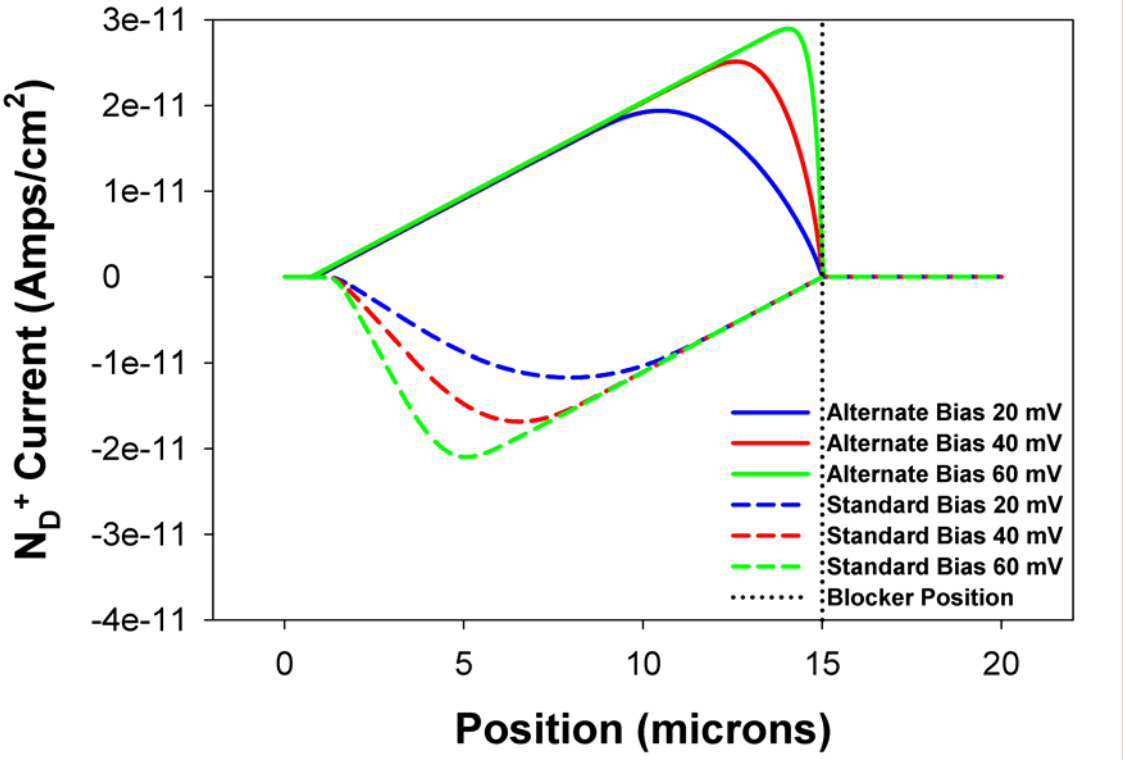

Figure 11. Hopping Current as a Function of Position for multiple Bias Voltages.

Figure 11 displays the hopping current for standard and alternate bias configurations. For standard bias operation, Figure 11 depicts the current created by the ionized donors N_D^+ moving outside the depletion region. The ionized donors which move outside of the depletion region recombine with free carriers present near the active layer contact. This prevents the build up of hopping currents near the contact. At the same time, the blocking layer prevents re-introduction of ionized donors into the depletion region of the device and restricts the overall contribution of the hopping current. Note that the magnitudes of the currents in Figure 11 are several orders of magnitude lower than in Figure 10. For alternate bias operation, the figure shows that the blocking layer prevents the current from the ionized donors from reaching the blocking layer contact. In this case, the extremely low mobility of the high purity blocking layer prevents the electrons that make up the hopping current from passing through

the blocking layer. These electrons are confined to the dopant band and cannot complete the circuit through the device.

The change of polarity required to create an alternate bias mode affects the free carriers that reside in the each of device's contacts. An examination of diffusion currents will show that these free carriers do not contribute to the detector's photocurrent regardless of the bias modes. When a standard bias is applied to a detector, the free carriers present in the blocking layer contact migrate out of the detector and have no significant effect on the device operation. The free carriers present in the active layer contact diffuse into the active layer of the device; however, this diffusion is limited by the compensation doping present in the active layer. Figure 12 depicts the effects of near contact diffusion on the electric field profile.

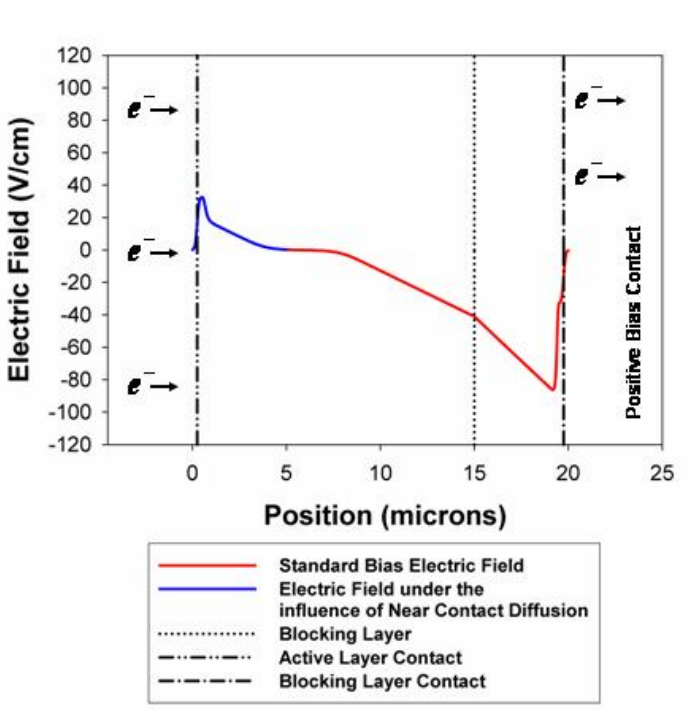

Figure 12. The Effects of Near-Contact Diffusion on the Electric Field (Standard Bias).

Known as the Debye tail, the carrier diffusion affects a relatively small portion of the device and its effects terminate prior to reaching the depletion region of the device. Near contact diffusion is discussed in detail within the next section. The alternate bias configuration forces a similar reaction by both contacts' free carriers. When applying an alternate bias to a device, the free carriers in the active layer contact migrate out of the device and do contribute to device operation. The free carriers in the blocking layer contact of the device diffuse into the blocking layer of the device. If the blocking layer is sufficiently thick, these carriers fail to pass through the blocking layer and will not affect the depletion region of the device. The direction of free carriers' diffusion along with the resulting Debye tail is depicted in Figure 13. A detailed analysis of drift and diffusion currents is provided in the next chapter. In the near contact region, both drift and diffusion can play important roles in determining the net current. Because the blocking layer serves as the injecting contact in an alternate bias BIB, it is necessary to take a detailed look at carrier dynamics in the blocking layer.

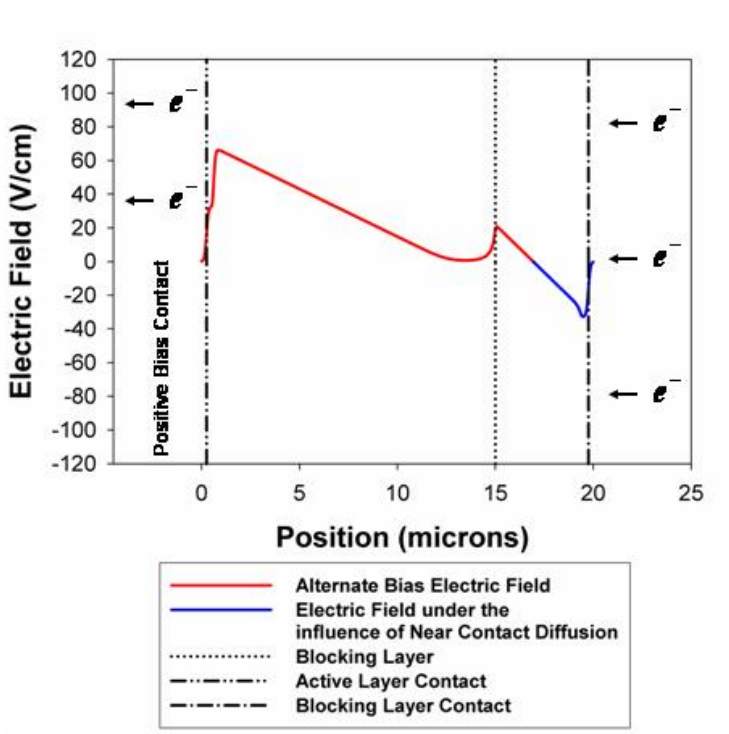

Figure 13. The Effects of Near-Contact Diffusion on the Electric Field (Alternate Bias).

B. DIFFUSION CURRENTS

Within the BIB computer model, the ohmic contacts are treated as heavily doped layers, whose dopant concentrations grade into both the active and blocking layers of the device. These contacts are degenerate and contain a free carrier concentration that is in excess of the Mott transition, which allows for diffusion into the adjacent layers of the device, at all temperatures. This phenomenon is known as near-contact diffusion and was discussed in detail for Ge:Ga and Si:As photoconductors by C.S. Olsen et al. in a paper published in 1993 [23]. The extent of this free carrier diffusion into the blocking or active layer of the device depends on the concentration of minority dopant. The compensation provides for ionized donors N_D^+, which trap the negatively charged free carriers and prevent any further intrusion into the adjacent layer. As the free carriers diffuse into the adjacent layer, they produce both current and an

opposing electric field. As discussed in an early section this electric field is known as a Debye tail. Because of these relationships, a higher compensation level in either the active or blocking layers of the device will limit diffusion lengths, which produces a smaller Debye tail.

To understand the carrier dynamics within a BIB device, it is important to examine the spatial variation of the currents that were caused by near-contact diffusion. To accomplish this task, the model allows for the calculation of the individual components of the total photocurrent. In the near-contact region, diffusion and drift represent the dominant sources of current. The diffusion current is represented by,

$$J_{Diffusion} = \mu kT \frac{\partial n}{\partial x} \qquad (3.2)$$

where μ is the bulk material's mobility, k is the Boltzmann constant, T is the temperature, and n is the concentration of electrons present. Figure14 shows the calculated diffusion current profile for a GaAs detector (Table 3) that is employing the standard bias mode. Under standard bias mode, the free carriers in the active layer's contact move into the active layer of the device, which creates both current and an opposing electric field. This free carrier migration creates current that is moving towards the blocking layer contact and is represented by the blue line in Figure 14. As the free carriers move into the device, they interact with any ionized donors present which forces the current and electric field to decay. Outside of the Debye tail, any changes in the diffusion current profile within the device reflect minor changes in the electron distribution. Since bias is applied to the blocking layer contact, the Debye tail is shorter in the blocking layer. This diffusion of current moves towards the active layer and is depicted by the short red line in Figure 14.

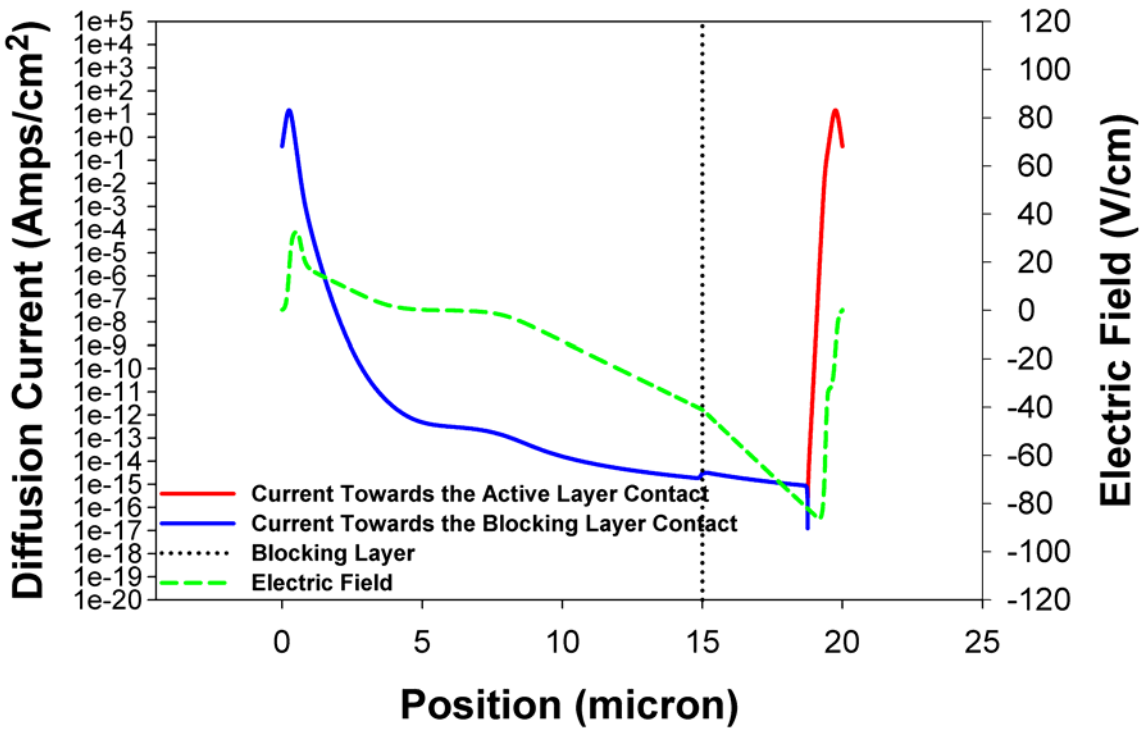

Figure 14. Diffusion Currents as a Function of Position for the Standard Bias Mode.

Figure 15 shows the diffusion current for the same GaAs detector; however, the alternate bias mode is now applied. Since positive voltage is applied to the active layer contact, the near contact diffusion in the active layer is less extensive. This current moves towards the blocking layer, which is represented by the blue line. The small changes in diffusion current within the active layer of the device reflect variations in the detector's electron distribution. When approaching the blocking layer, the direction of current experiences a change that is consistent with the changes in dopant at the blocking layer to active layer interface. The diffusion current in the blocking layer is influenced by both near-contact diffusion and the applied voltage. The low levels of compensation in the blocking layer allow for an extended Debye tail within this region of the device. The applied voltage at the active layer contact promotes the extension of the Debye tail further into the blocking layer. Because of this

increase in diffusion lengths, alternate bias mode BIB detectors may require thicker blocking layers. The thicker blocking layer will ensure that the Debye tail remains isolated from the depletion region of the device. This isolation prevents the blocking layer contact from saturating the detector with free carriers. The ramification of creating thicker blocking layers is discussed in the next chapter. The currents depicted in Figure 14 and 15 demonstrate several important aspects for BIB operation that occur regardless of bias mode. First, the large amount of diffusion current present at each of the contacts must be negated by drift current. The interaction of drift and diffusion currents will allow for the total current flowing within the device to remain constant. Once the currents present at the contacts have been balanced, the diffusion does not contribute in large amounts to the total photocurrent. Once these facts are understood, it becomes important to study drift currents in order to completely understand the carrier dynamics of these devices.

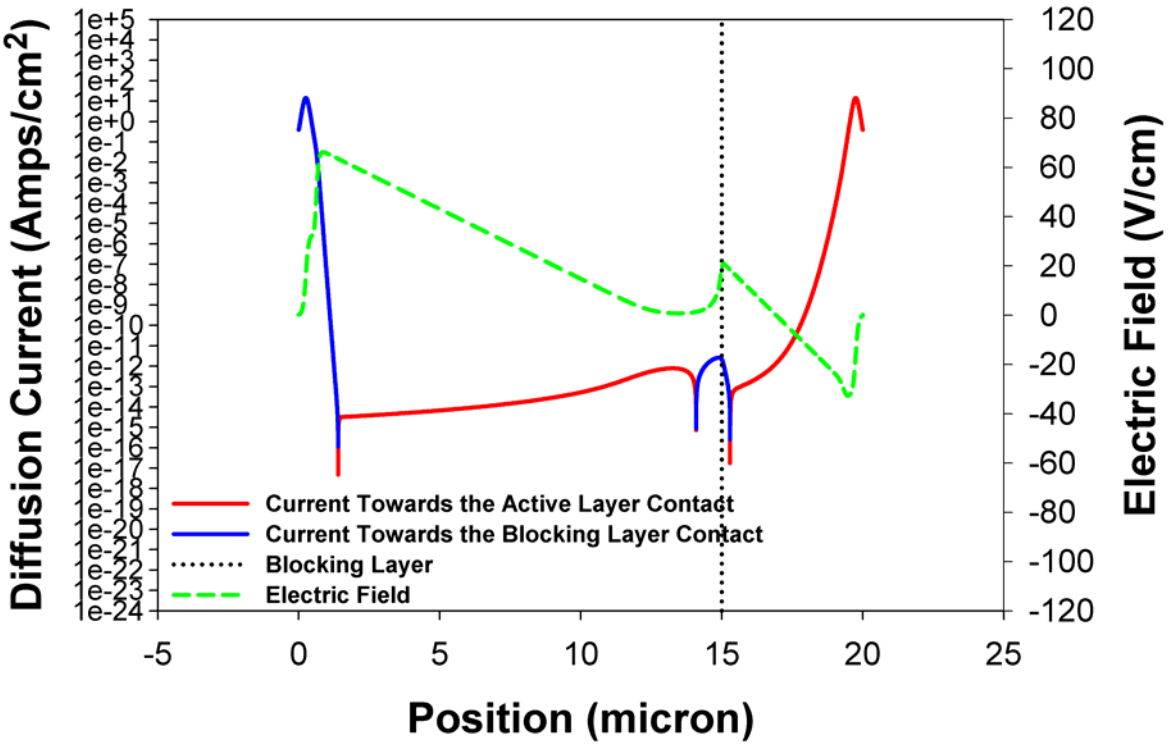

Figure 15. Diffusion Currents as a Function of Position for the Alternate Bias Mode.

C. DRIFT CURRENTS

An examination of the drift currents was conducted in order to understand the carrier transport in the near-contact regions for both bias modes. Representing the dominant component of the total photo-current, the drift current is given by

$$J_{Drift} = ne\mu E_x \tag{3.3}$$

where n is the concentration of electrons, e is the fundamental charge, μ is mobility, and E_x is the magnitude of the electric field as a function of position. Figure 16 shows the drift current profile for the fore-mentioned GaAs detector, while operating under the standard bias mode. The electric field created by the near-contact diffusion at the active layer contact creates a drift current back towards the contact, which is represented by the positive values (red line) in Figure 16. At the same time, the negative values (blue line) represent drift current moving towards the blocking layer contact. This current is under the influence of the depletion region's electric field. The large amount current present at each contact is negated by a large amount of diffusion current moving in the opposite direction, which is represented in Figure 16. The two currents present at the contacts counter-act and ensure that total current remains constant throughout the entire BIB detector. When an alternate bias mode is applied to the same detector, similar results are produced. In this case, the depletion region and its associated electric field are created solely in the active layer of the device. This electric field drives the drift current towards the active layer contact and is depicted by the red line in Figure 17. At the same time, the electric field that was created by the near-contact diffusion in the blocking layer forces the drift current in the opposite direction. The combination of drift and diffusion currents ensure that the total photocurrent remains constant across the device. This balance between drift and diffusion currents ensures that the free carriers in the contacts do not saturate the device.

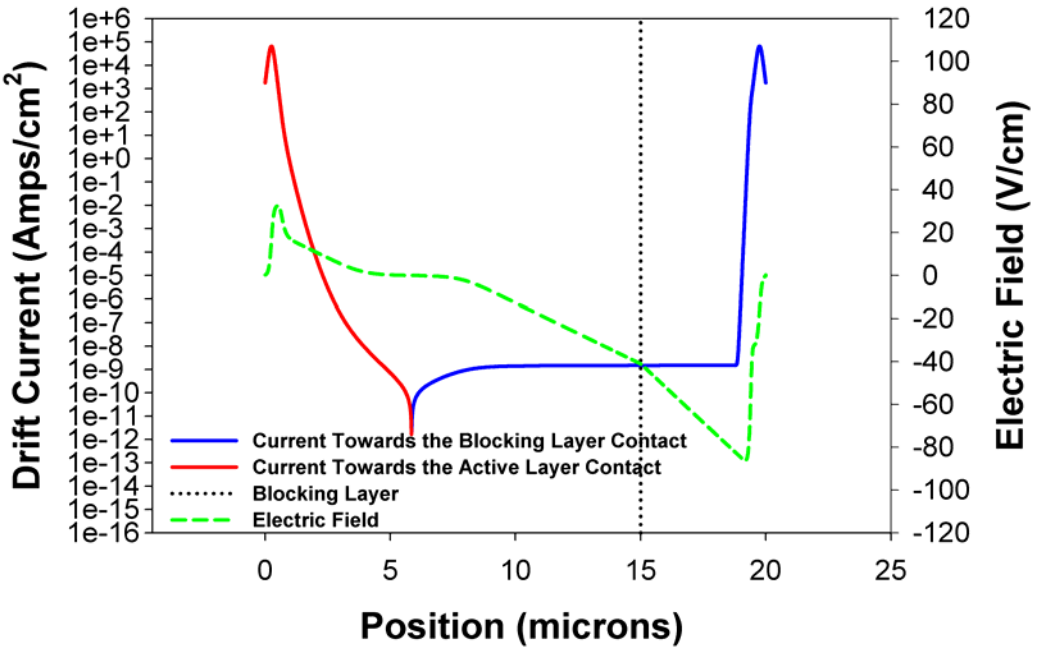

Figure 16. Drift Current as a Function of Position for a Standard Bias BIB Detector.

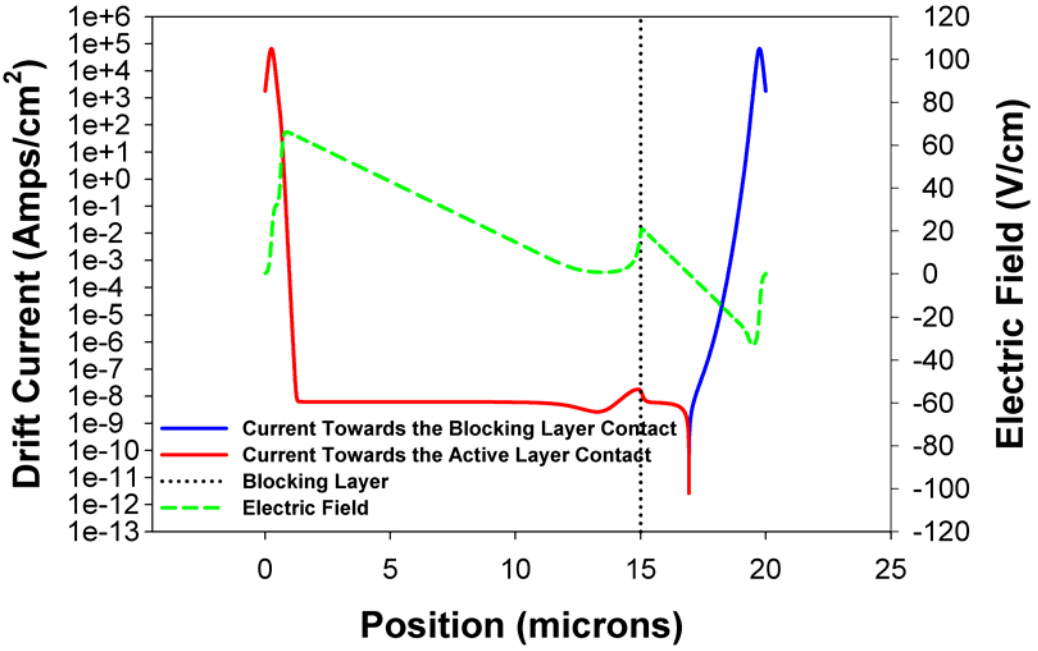

Figure 17. Drift Current as a Function of Position for an Alternate Bias BIB Detector.

IV. MODELING AND SIMULATION RESULTS

A. SIGNAL TO NOISE RATIO OF BOTH BIAS MODES

The results from Chapter III detail a comparison between the depletion regions created by alternate and standard bias modes. Figure 9 shows that the alternate bias mode produces a greater depletion region for a given voltage and creates more current. These results raise the following question: Is the increase in current demonstrated by the alternate bias mode only a product of increased dark or hopping current levels? In order to answer this question, a series of simulations were conducted to determine the Signal to Noise Ratio (SNR) of both bias modes. Table 4 summarizes the parameters utilized to simulate a Si detector under varying bias conditions.

Absorbing Layer Majority Doping	2.0×10^{17} cm^{-3}
Absorbing Layer Minority Doping	1.0×10^{13} cm^{-3}
Absorbing Layer Thickness	4 μm
Blocking Layer Majority Doping	1.0×10^{12} cm^{-3}
Blocking Layer Minority Doping	1.0×10^{11} cm^{-3}
Temperature	4 K
Applied Bias	0, $\pm$150, $\pm$300, $\pm$450, $\pm$600, $\pm$750, $\pm$900, $\pm$1050, $\pm$1200 mV
Bohr Radius	15×10^{-10} m
Interface grade parameter	2.0×10^{-7} cm
Contact grade parameter	1.0×10^{-5} cm
Optical flux rate γ	5.0×10^{-7} s^{-1} for Photo-Current 5.0×10^{-10} s^{-1} for Dark Current

Table 4. Si Modeling Parameters.

Three important characteristics of this experiment must be explained. First, the modeling can only approximate the photon limited shot noise that is present in the detector. There are no mechanisms in the model for contact noise or any noise that might be associated with supporting electronics. Second, Si detectors were utilized because their modeling parameters allow for significantly lower simulation times when compared to those of a GaAs detector. At the same time, Si BIBs represent a majority of the available experimental data that could be employed for further detector characterization. Lastly, the optical flux rate γ

was set to 5.0 x 10^{-10} s^{-1} when examining dark current cases due to limitations in the BIB computer program. Attempts to lower the optical flux rates resulted in extremely long simulation run times or numerical underflows within the BIB simulation computer program. Under absolute zero light conditions, the thermal current is too small to calculate numerically, so a low value of γ was used to simulate a fixed dark current and/or background flux. Figures 18, 19 and 20 show the results of these simulations.

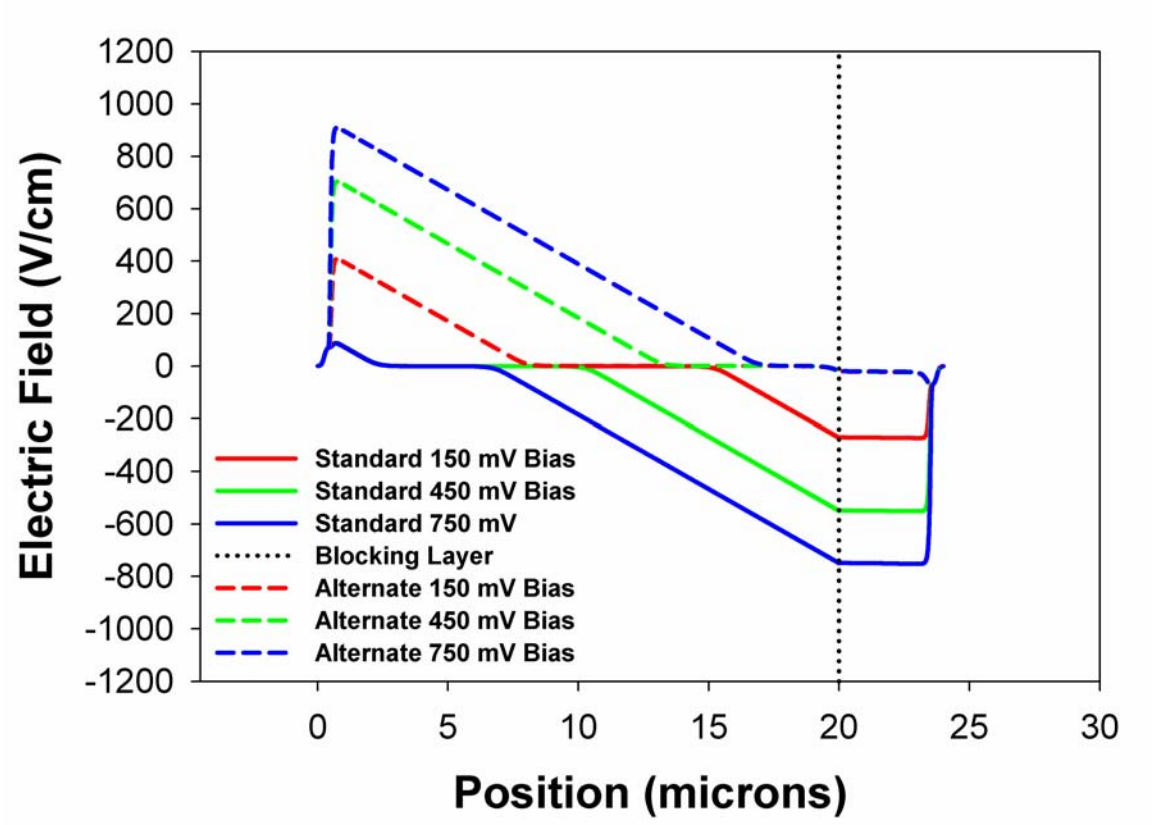

Figure 18. Electric Field as a Function of Position for Various Applied Bias.

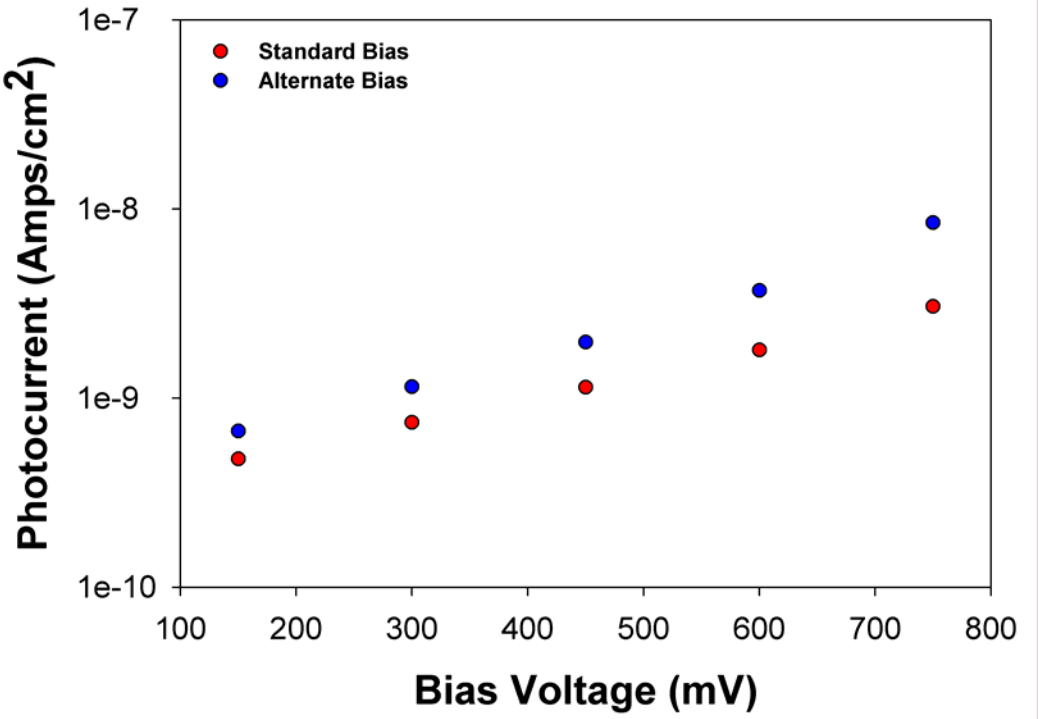

Figure 19. Photocurrent as a Function of Applied Bias.

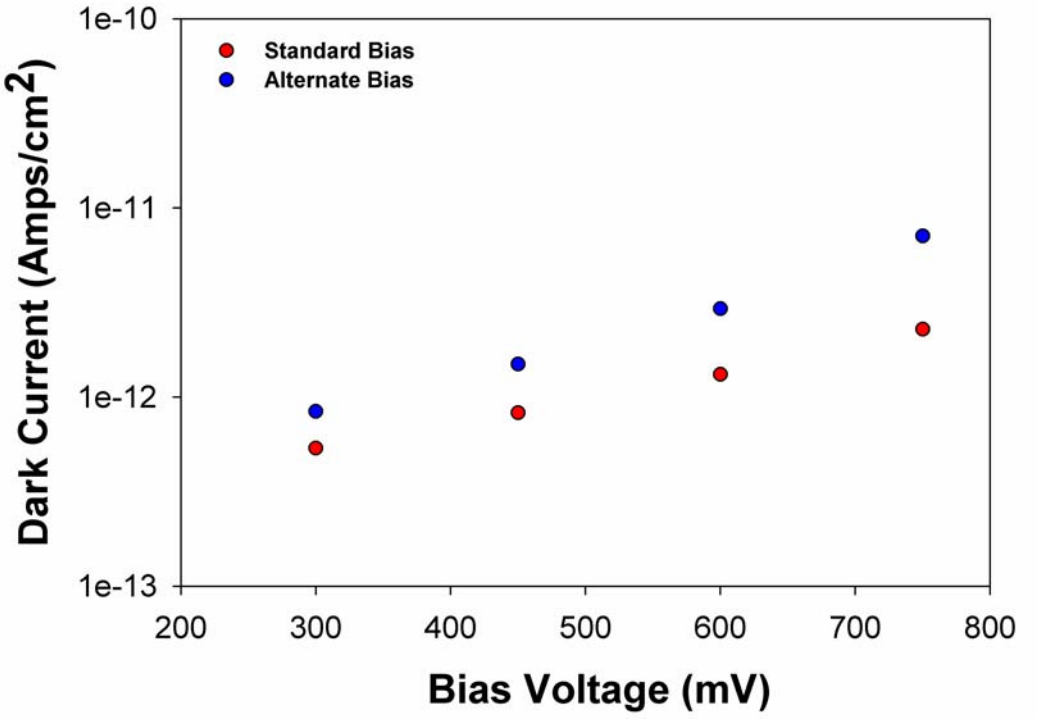

Figure 20. Dark Current as a Function of Applied Bias.

Figure 18 depicts several of the electric fields as a function of position for varying bias. Mirroring the results seen earlier for a GaAs detector, the alternate bias mode provides for a larger depletion region within the active layer of the device. The larger depletion regions provide for a greater amount of total photocurrent, which is plotted as a function of bias in Figure 19. Similarly, the alternate bias mode creates a larger amount of dark current, which is shown in Figure 20. It is important to remember that dark current is a combination of thermally generated current and hopping current. In order to compare the performance of the bias modes, the SNR was calculated through

$$SNR = 20\log\left(\frac{TPC}{\sqrt{2eB(DC)}}\right) \tag{4.1}$$

where TPC is the total photocurrent (Figure 19), B is the bandwidth of the detector, e represents the fundamental charge of an electron, and DC is the dark current (Figure 20) [24]. In this case, B was set to 1 Hz. Figure 21 shows that the alternate bias mode provides a larger SNR, which increases the detector's overall desirability.

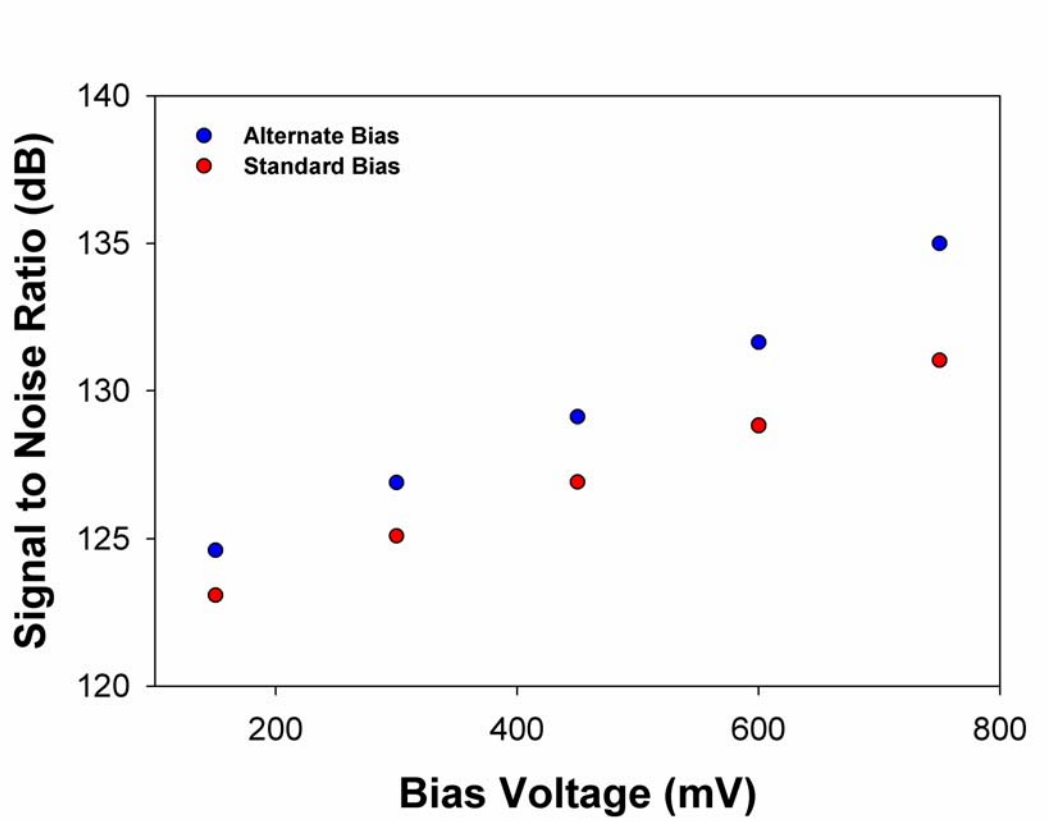

Figure 21. SNR as a Function of Applied Bias for Conditions of Table 4.

The increase in performance experienced through the use of the alternate bias mode is the result of device asymmetries. An increase in applied bias does not result in equal increases in the current produced by the two modes of operation. This phenomenon is depicted in Figure 22. Ultimately, the amount of photocurrent and dark current produced by a BIB detector depends on the size of the depletion region and the amount of applied bias. Since the total photocurrent grows faster than the square root of the dark current when applied bias is increased, the SNR improves for higher biases. The asymmetric nature of the device may provide options to circumvent limitations associated with the production of BIBs.

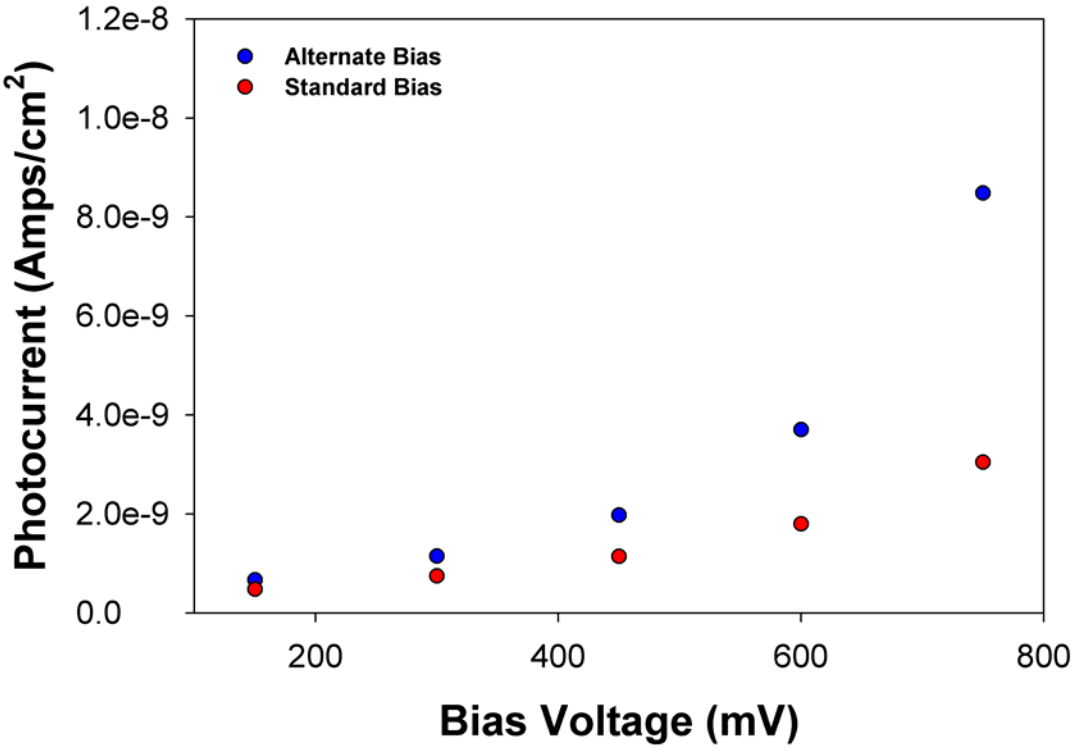

Figure 22. Photocurrent as a Function of Applied Bias Utilizing a Linear Scale.

B. BLOCKING LAYER THICKNESS

Despite the success of the Si based BIB detectors, the introduction of longer wavelength Ge and GaAs detectors has been delayed due to limitations in LPE growth techniques. Unfortunately, near equilibrium LPE growth techniques allow for the diffusion of doping materials across the blocker-active layer interface. This phenomenon could create a situation where the blocking layer becomes contaminated with dopant and does not reach the desired level of purity and resistance. Creating a thicker blocking layer represents the simplest solution to this problem. In order to fully understand the consequences of creating a thicker blocking layer, a series of simulations were completed covering the detector characteristics depicted in Table 5.

Absorbing Layer Majority Doping	2.0×10^{17} cm^{-3}
Absorbing Layer Minority Doping	5.0×10^{12} cm^{-3}
Absorbing Layer Thickness	20 μm
Blocking Layer Majority Doping	1.0×10^{12} cm^{-3}
Blocking Layer Minority Doping	1.0×10^{11} cm^{-3}
Blocking Layer Thickness	4 μm, 6 μm, 8 μm
Temperature	4.2 K
Applied Bias	0, ±150 , ±300, ±450, ±600, ±750, ±900 mV
Bohr Radius	15×10^{-10} m
Interface Grade Parameter	2.0×10^{-7} cm
Contact Grade Parameter	1.0×10^{-5} cm
Optical Flux Rate γ	5.0×10^{-7} s^{-1}

Table 5. Si BIB Modeling Characteristics for Varying Blocker Thickness.

A BIB detector employing the standard bias mode requires a relatively thin blocking layer in order to maintain the detector's efficiency. As discussed in Chapter I, the width of the depletion region can be analytically approximated by

$$w = \left[\frac{2\kappa_o \varepsilon_o}{qN_A} |V_b| + t_B^2 \right]^{1/2} - t_B \qquad (4.2)$$

where w is the width of the depletion region, V_b is the bias voltage, N_A is the density of the ionized acceptors, κ_o is the dielectric constant of the active layer material, ε_o is the permittivity of the active layer material, and t_B is the blocking

layer thickness [25]. This analytic expression clearly shows that the width of the depletion region depends directly upon the blocker thickness. By increasing blocker thickness, a BIB detector employing the standard bias mode creates a smaller depletion region, which produces a smaller photocurrent across all ranges of applied bias. The area under the electric field in the blocker represents a net voltage drop. These results are seen in Figures 23 and 24.

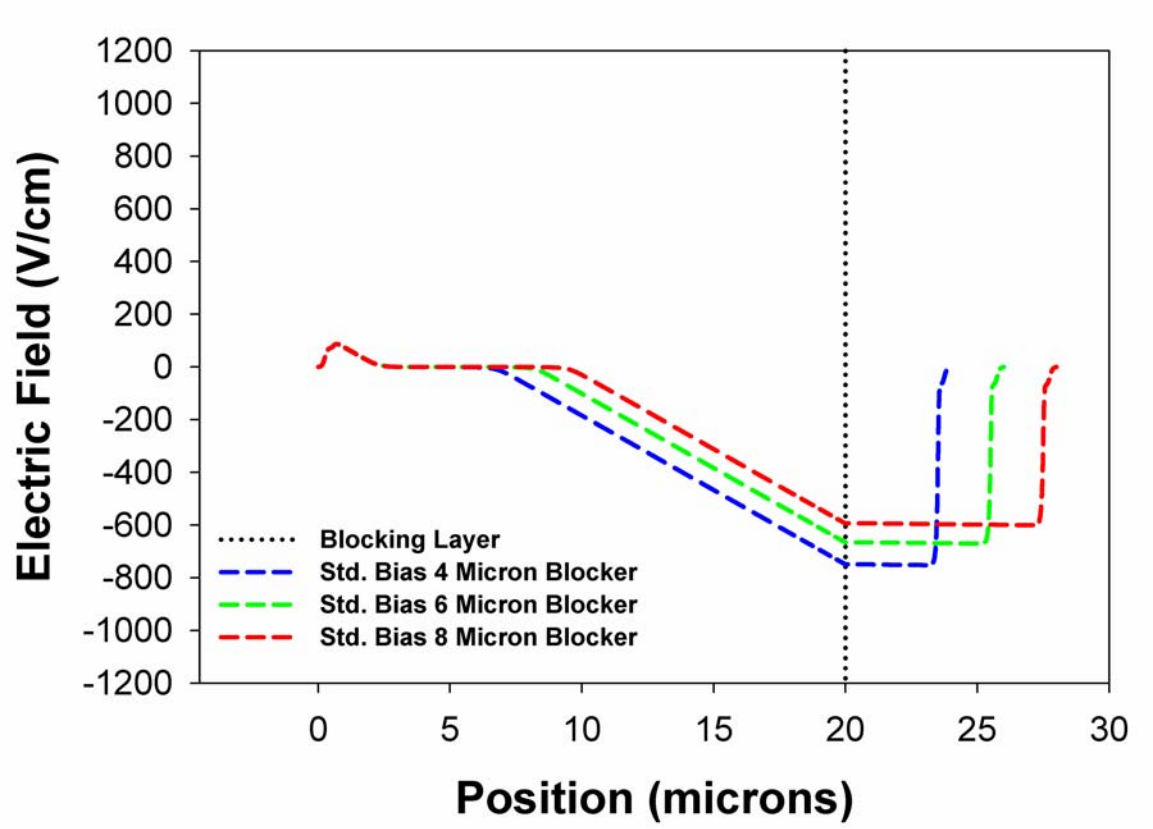

Figure 23. Electric Field as a Function of Position for Various Blocker Thicknesses with a Constant 750 mV Bias.

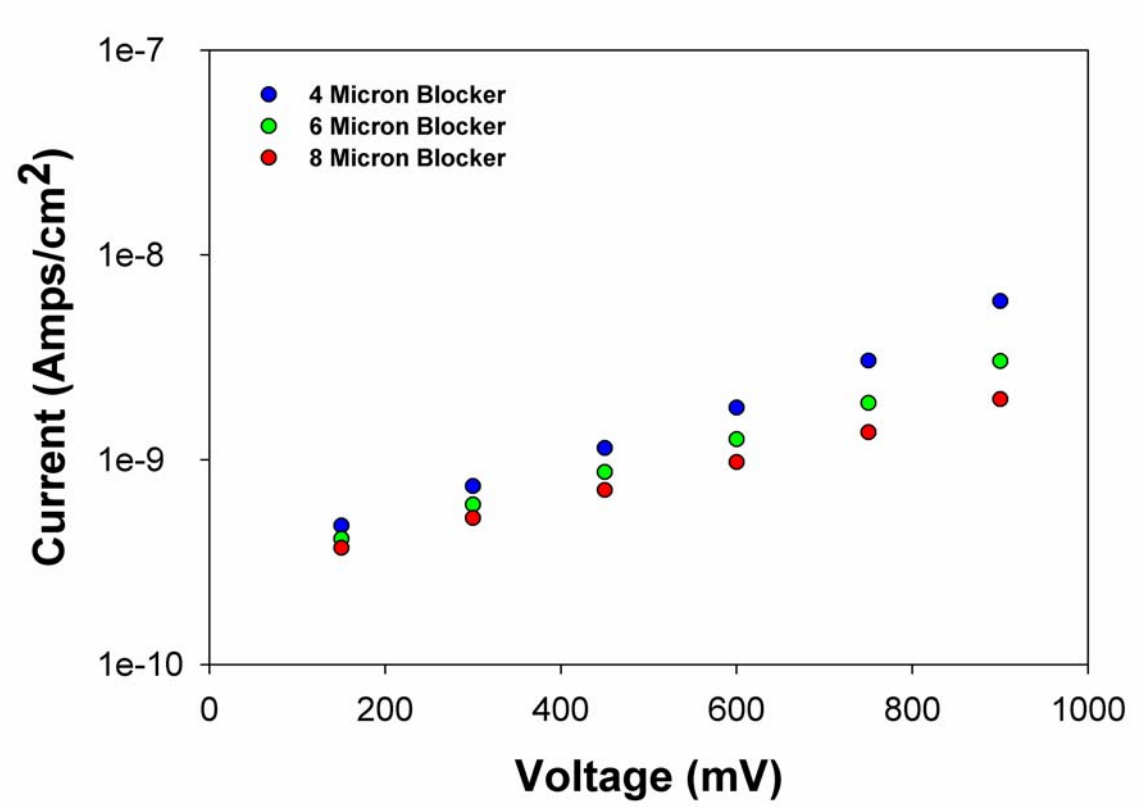

Figure 24. Current as a Function of Bias Voltage for Various Blocker Thicknesses.

Throughout the earlier chapters, the figures and analysis provided show that the alternate bias mode isolates the blocking layer from the depletion region of device. These results are clearly seen in Figures 9 and 18. Since the electric field is much lower and the bias voltage is no longer dropped in large amounts across the blocking layer, the amount of current created by the alternate bias mode is only very weakly dependent on the blocker thickness. Figures 25 and 26 illustrate these results. Note that the width of the depletion region in Figure 25 is virtually independent of variations in blocker thickness.

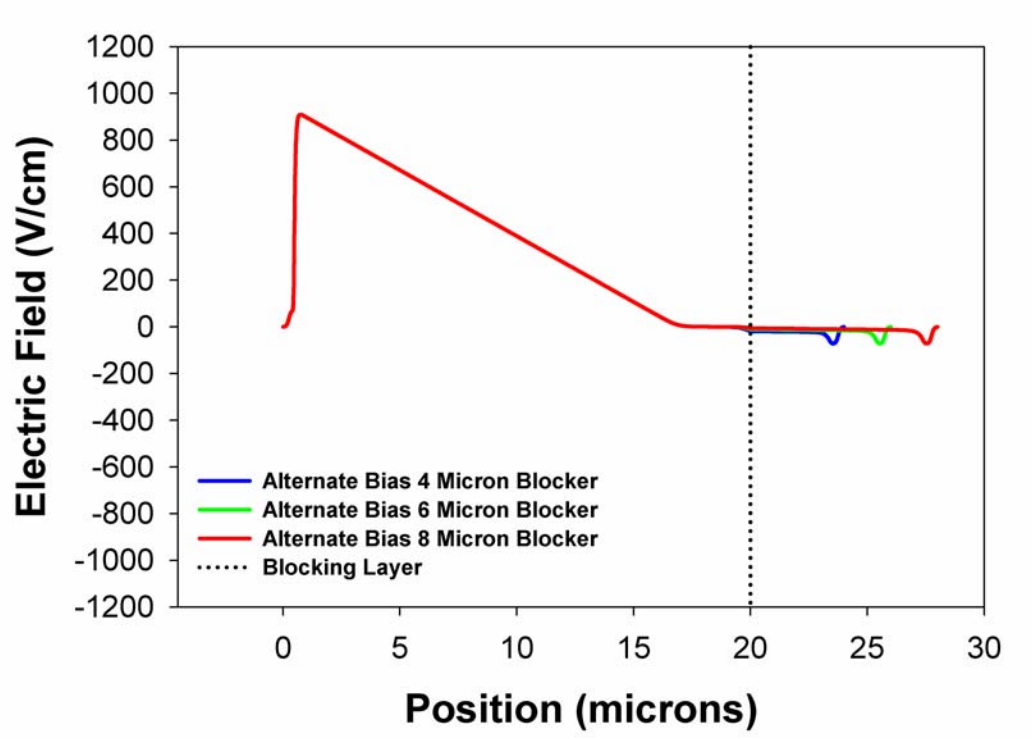

Figure 25. Electric Field as a Function of Position for Various Blocker Thicknesses with a Constant 750 mV Bias.

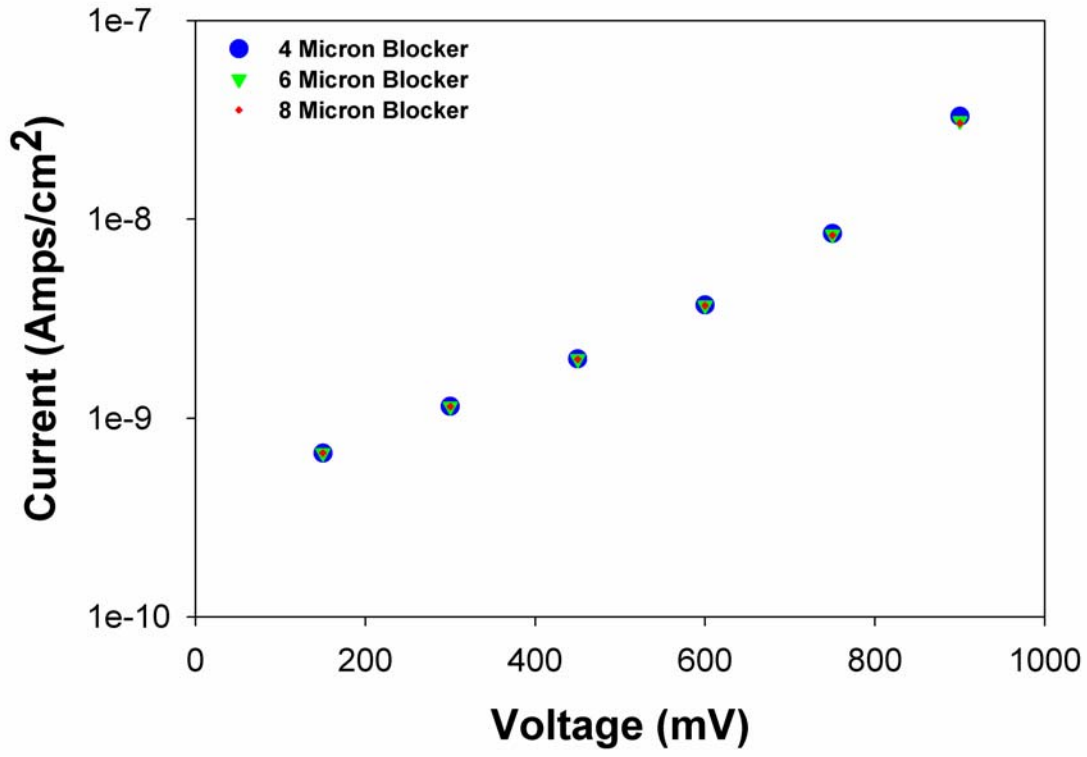

Figure 26. Current as a Function of Bias Voltage for Various Blocker Thicknesses.

Comparing Figures 24 and 26 shows that increasing blocker thickness produces greatly divergent results for the two operating modes. When employing the standard bias mode, an increase in blocker thickness decreases the amount of photocurrent produced by the device for a given voltage. At the same time, an increase in blocker thickness produces only slight changes in the available photocurrent when operating under the alternate bias mode. This conclusion is quantified in Table 6. In this table, the data have been normalized to the current that is produced by a 150 mV standard bias acting on a detector with a 4 micron blocker. The effect of increasing blocker thickness at 150 mV illustrates these conclusions. In standard bias mode, the detector loses 22% of its photocurrent when the blocker thickness is increased from 4 microns to 8 microns. In the alternate bias mode, the amount of photocurrent produced remains the same regardless of the blocker thickness.

	Blocker Thickness		
	4 micron	6 micron	8 micron
Standard Bias			
150 mV	1.00	0.86	0.78
450 mV	2.39	1.83	1.49
750 mV	6.39	3.98	2.86
Alternate Bias			
150 mV	1.40	1.40	1.40
450 mV	4.15	4.13	4.13
750 mV	17.79	17.51	17.39

Table 6. Normalized Photocurrent in Comparison to Blocker Thickness.

Building upon the methodology employed in Chapter III to calculate the Signal to Noise Ratio, Table 7 quantifiably shows that operating under alternate bias modes allows for the use of thicker blockers without suffering significant performance degradation. Despite the reduced role that the blocker thickness plays in alternate mode configurations, it is important to remember that increasing overall device thickness tends to reduce some of the inherent advantages of the device. For instance, a larger device increases the volume of the detector and makes it more vulnerable to radiation damage. The issues governing overall detector performance would preclude the employment of

extravagantly thick detectors. At the same time, the alternate bias mode produces a situation where an increased photocurrent signal is produced with less voltage, which reduces both the power and cooling requirements assigned to the detector design. These are important factors in detector use on cryogenic space platforms, where both power and cooling are valuable resources. Ultimately, BIB detectors employing an alternate bias configuration require further analysis to determine optimal device performance.

	Blocker Thickness		
	4 micron	6 micron	8 micron
Standard Bias			
150 mV	124.61 dB	124.61 dB	124.61 dB
450 mV	129.11 dB	129.10 dB	129.10 dB
750 mV	135.00 dB	134.94 dB	134.91 dB

Table 7. Signal to Noise Ratios in Comparison to Blocker Thickness for the Alternate Bias Mode.

V. CONCLUSIONS

A. CONCLUSIONS

To further extend BIB detector coverage into the 40-350 μm range, Ge and GaAs BIB detectors are required. Unfortunately, the introduction of these new detectors has been delayed due to growth and fabrication limitations. These limitations include the inability to grow either a sufficiently thin high purity blocking layer or an efficient blocking to active layer interface. Numerical modeling shows that an alternate bias mode exists for BIB detectors that minimizes these fabrication issues. The computer simulations demonstrate that the alternate bias mode allows for the creation of a depletion region exclusively in the active layer of the device. The creation of a depletion region in this manner allows for the isolation of the blocking to active layer interface, which minimizes the impact of any grading between the two layers. Since minimal voltage is lost across the blocking layer, the alternate bias mode creates a wider depletion region. Because of these factors, devices employing the alternate bias mode generate more total photocurrent than those using the standard bias mode. The currents created by both modes of operation for several applied biases and two different optical generation rates were calculated in order to determine the SNR of both BIB configurations. The alternate bias mode consistently produced a larger SNR, which highlights the asymmetries between the different bias modes.

To determine the feasibility of fielding an alternate bias mode BIB detector the internal detector transport was examined. The modeling shows that the blocking layer still effectively prevents hopping currents from reaching the appropriate contact, which preserves the benefits associated with this multi-layered device. The inherent strengths of the computer simulation allow for the examination of near contact diffusion and its effect upon device operation. The heavily doped ohmic contacts produce drift and diffusion currents within the device. Examinations of these two different components of current shows that

the free carriers present in the two ohmic contacts do not saturate the device. Near contact diffusion along with LPE growth considerations make thicker blocking layers more desirable.

B. FUTURE WORK

The work compiled in this thesis provides the basic operational theory of BIB detectors employing an alternate bias mode; however, much work remains. To further this endeavor, improvements to the BIB computer suite, continued modeling, and experimental work are required. The computational suite can be improved through the introduction of a 64 bit operational system, which would allow for the utilization of improved FORTRAN compilers and mathematical libraries. These efforts ensure that the computer model remains supportable with current technology, while possibly improving computational speeds. At the same time, the establishment of file sharing between the individual computers would significantly reduce the amount of time required to manipulate output data, while reducing the organizational requirements associated with the storage of historical lab data files. The introduction of advanced high performance computer measures such as parallel super computing would represent the apex of the existing BIB computer suite. This could be accomplished through the employment of a Class I Beowulf Cluster, which would take advantage of the commercial technology employed in the lab. A Beowulf Cluster would greatly reduce the run time of any simulation and provide the computational power necessary for any new modeling capabilities that is desired. The improvements suggested in this chapter do not require any additional hardware, but do involve an investment in new software.

The inherent flexibility of the computer model allows for further studies into feasibility of fielding alternate bias mode BIB detectors. An examination of the effects of non-optimal dopant and compensation concentrations upon detector performance is required. Because of the effects of near contact diffusion in the blocking layer, modeling is required to determine the consequences of creating significantly wider blocking layers upon overall detector performance and the mechanisms for current injection through the blocker while in an alternate bias

mode. These studies would continue the efforts to find detector configurations that reduce the effects of LPE growth limitations upon the introduction of GaAs and Ge devices. Ultimately, the modeling could provide a detector configuration that is achievable with current manufacturing techniques. Despite any insights gained through the modeling of BIB detectors, the fielding of an alternate bias mode detector depends upon substantial experimental work.

In order to convince the far infrared detector community of the viability of an alternate bias mode BIB device, significant experimental work is required. This work would include the fabrication and characterization of a BIB device specifically created for alternate bias mode operation. Once a detector was created, the photo-response could be measured and compared to the modeling results. Prior to the completion of this thesis, researchers from the Naval Post Graduate School and the University of California Berkeley have begun collaborative efforts to fabricate and test an alternate bias mode BIB device. In the end, these efforts will determine if an alternate bias mode BIB represent a solution for high sensitivity, radiation hard, large format array detection in the 40 to 350 μm range.

THIS PAGE INTENTIONALLY LEFT BLANK

LIST OF REFERENCES

1. Petroff, M. D. and Stapelbroek M. G., US Patent No 4,568,960 (4 February 1986).
2. Szmulowicz, F. and Madarsz, F. L., “Blocked Impurity Band detectors-An analytical model: Figures of merit,” *Journal of Applied Physics*, **62**, 2534, 1997.
3. Nalwa, Hari Singh. *Photodetectors and Fiber Optics*. (San Diego: Academic Press, 2001), 70.
4. Haegel, N. M., “Photoconductors for 200-400 μm: choices and challenges.” *Nuclear Instruments and Methods in Physics Research*, **377**, 501, 1996.
5. Haegel, N. M., “Photoconductors for 200-400 μm: choices and challenges.” *Nuclear Instruments and Methods in Physics Research*, **377**, 503, 1996.
6. Reichertz, L.A., Beeman, J. W., Cardozo, B. L., Haegel, N. M., Haller E. E., Jakob, G., Katterloher, R., “ GaAs BIB photodetector development for far-infrared astronomy,” *SPIE*, **5543**, 231-238, 2004.
7. Reichertz, L.A., Beeman, J. W., Cardozo, B. L., Haegel, N. M., Haller E. E., Jakob, G., Katterloher, R., “ GaAs BIB photodetector development for far-infrared astronomy,” *SPIE*, **5543**, 231-238, 2004.
8. Bardaru, J., Beeman, J. W., Haller, E. E., Samperi, S., Haegel, N.M., “Influence of the Sb dopant distribution on far infrared photoconductivity in Ge;Sb blocked impurity band detectors,” *Infrared Physics and Technology*, **43**, 357, 2002.
9. Huffman J.E., Crouse A.G., Halleck B.L., Downes T. V., Herter T. L., “Si:Sb blocked impurity band detectors for infrared astronomy,” *Journal of Applied Physics*, **72**, 273, 1992.
10. Watson D. M. and Huffman, J. E., “Germanium blocked-impurity-band far-infrared detectors.” *Applied Physics Letters*, **52**, 1602, 1988.
11. Rieke, G. H., *Detection of Light: From the Ultraviolet to the Submillimeter*. (Cambridge: Cambridge University Press, 1994), 97.

12. Haegel, N. M., Samperi, S. A., White, A. M., “Electric field and responsivity modeling for far-infrared blocked impurity band detectors,” *Journal of Applied Physics*, **93**, 1306, 2003.
13. Haegel, N. M., Schwartz, W. R., Zinter, J., White, A. M., Beeman, J. W., “Origin of the hook effect in extrinsic photoconductors”, *Applied Optics*, **40**, 5748-5754, 2001.
14. Haegel, N. M., Grennan C. R., White, A. M., “Transport in extrinsic photoconductors: a comprehensive model for transient response”, *Journal of Applied Physics*, **80**, 1910-1919, 1996.
15. White, A. M., “Numerical Analysis of Extrinisic Detectors,” Personal Correspondence, January 2004.
16. White, A. M., “Numerical Analysis of Extrinisic Detectors,” Personal Correspondence, January 2004
17. White, A. M., “Numerical Analysis of Extrinisic Detectors,” Personal Correspondence, January 2004
18. White, A. M., “Numerical Analysis of Extrinisic Detectors,” Personal Correspondence, January 2004
19. Haegel, N.M., Jacobs, J.E., White, A.M., “Modeling of steady-state field distributions in blocked impurity band detectors,” *Applied Physics Letters*, **77**, 4389, 2000.
20. Haegel, N. M., Samperi, S. A., White, A. M., “Electric field and responsivity modeling for far-infrared blocked impurity band detectors,” *Journal of Applied Physics*, **93**, 1306, 2003.
21. Haegel, N.M., Jacobs, J.E., White, A.M., “Modeling of steady-state field distributions in blocked impurity band detectors,” *Applied Physics Letters*, **77**, 4389, 2000.
22. Haegel, N. M., Samperi, S. A., White, A. M., “Electric field and responsivity modeling for far-infrared blocked impurity band detectors,” *Journal of Applied Physics*, **93**, 1307, 2003.

23. Olsen, C.S., Haegel, N.M., White, A.M., Huffman, J.E., Kinoshita, F.F., Beeman J.W., “Near-Contact Diffusion and Compensation in Extrinsic Photoconductors,” *Infrared Physics*, **34**, 61-66, 1993.

24. Dereniak, E. L., and Boreman G.D., *Infrared Detectors and Systems.* (New York: John Wiley and Sons, Inc, 1996) 197.

25. Rieke, G. H., *Detection of Light: From the Ultraviolet to the Submillimeter*. (Cambridge: Cambridge University Press, 1994), 97.

THIS PAGE INTENTIONALLY LEFT BLANK

INITIAL DISTRIBUTION LIST

1. Defense Technical Information Center
   Ft. Belvoir, VA

2. Dudley Knox Library
   Naval Postgraduate School
   Monterey, CA

3. Professor Nancy M. Haegel
   Naval Postgraduate School
   Monterey, CA

4. Professor Gamani Karunasiri
   Naval Postgraduate School
   Monterey, CA

5. Professor James H. Luscombe
   Naval Postgraduate School
   Monterey, CA

6. Professor Eugene Haller
   University of California, Berkeley
   Berkeley, CA

7. Jeff Beeman
   University of California, Berkeley
   Berkeley, CA

8. Dr. Peter Love
   Raytheon Vision Systems
   Goleta, CA

9. Dr. Craig McCreight
   NASA AMES
   Moffett Field, CA